Effects of polymer polydispersity on the phase behaviour of colloid–polymer mixtures

2005 J. Phys.: Condens. Matter 17 797

(http://iopscience.iop.org/0953-8984/17/6/002)

INSTITUTE OF PHYSICS PUBLISHING JOURNAL OF PHYSICS: CONDENSED MATTER

J. Phys.: Condens. Matter **17** (2005) 797–812 doi:10.1088/0953-8984/17/6/002

Effects of polymer polydispersity on the phase behaviour of colloid–polymer mixtures

Moreno Fasolo and Peter Sollich

Department of Mathematics, King's College London, London WC2R 2LS, UK

E-mail: peter.sollich@kcl.ac.uk

Received 30 November 2004, in final form 6 January 2005
Published 28 January 2005
Online at stacks.iop.org/JPhysCM/17/797

Abstract

We study the equilibrium behaviour of a mixture of monodisperse hard sphere colloids and polydisperse non-adsorbing polymers at their θ-point, using the Asakura–Oosawa model treated within the free-volume approximation. Our focus is the experimentally relevant scenario where the distribution of polymer chain lengths across the system is fixed. Phase diagrams are calculated using the moment free energy method, and we show that the mean polymer size ξ_c at which gas–liquid phase separation first occurs decreases with increasing polymer polydispersity δ. Correspondingly, at fixed mean polymer size, polydispersity favours gas–liquid coexistence but delays the onset of fluid–solid separation. On the other hand, we find that systems with different δ values but the same *mass-averaged* polymer chain length have nearly polydispersity-independent phase diagrams. We conclude with a comparison to previous calculations for a semi-grand-canonical scenario, where the polymer chemical potentials are imposed; there it was found that fluid–solid coexistence was favoured over gas–liquid in some areas of the phase diagram. Our results show that this somewhat counter-intuitive result arose because the actual polymer size distribution in the system is shifted to smaller sizes relative to the polymer reservoir distribution.

1. Introduction

Colloid–polymer mixtures have a wide variety of practical uses: polymers can be added in low concentrations to colloidal suspensions to modify their properties [1–3], or conversely colloids can be added to polymer melts as 'fillers' [4] or to polymer solutions to produce gels [5]. In the former case, it is well known that the presence of the polymer can induce an effective colloid–colloid *depletion attraction* [6–9]. Unlike the case of atomic systems, both the strength and range of this interaction can be tuned by varying polymer concentration

and size. The implications of this for the phase behaviour of the mixture are of fundamental theoretical interest, and have been the subject of much research.

We focus on the simplest situation in this paper, where the colloids have hard interactions with each other and with the polymers; this requires in particular that the polymers be non-adsorbing on the surface of the colloids. We further restrict ourselves to θ-point conditions, where polymer–polymer interactions can be neglected to a first approximation. When the polymers are modelled as random walks on a lattice, this scenario is amenable to direct numerical simulation [10, 11]. However, most work has focused on a further simplification, proposed by Asakura and Oosawa (AO) [6, 7] and Vrij [8], where the polymers are replaced by spheres with radius equal to the radius of gyration of the original polymer chains. These 'polymer spheres' are then assumed to interpenetrate freely with each other while having a hard excluded volume interaction with the colloids. This AO model has been studied in great detail, by thermodynamic perturbation theory [12–14], free-volume theory [15] (see below), density functional theory [16–18], and Monte Carlo simulations [11, 19, 20]. Note that the naive choice of setting the radius of the effective polymer sphere equal to the polymer radius of gyration can be improved upon; we will return to this point in the discussion in section 4.

In addition to the simplifications already discussed, the AO model ignores the fact that there is, in real colloid–polymer mixtures, invariably an (essentially continuous) spread of polymer chain lengths. The effects of such *polymer size polydispersity* on the phase behaviour have been studied by some researchers. As described in more detail below, however, the experimentally relevant situation where the full polymer size distribution in the system is conserved during phase separation remains to be understood. This is the issue which we address in this paper. Specifically, we study the AO model within the free-volume approximation of [15], for the case where the colloids are monodisperse, with diameter σ_c, while the polymer spheres are polydisperse with density distribution $\rho_p(\sigma_p) = \rho_p n_p(\sigma_p)$. Here ρ_p is the polymer number density and $n_p(\sigma_p)$ is the normalized polymer diameter distribution. We take the colloid diameters σ_c as our unit of length so that the polymer-to-colloid diameter ratio ξ coincides with the dimensionless polymer diameter, $\xi \equiv \sigma_p$. All densities are made dimensionless by multiplying by the volume of a colloid particle, and quantities with the dimension of energy are measured in units of $k_B T$.

For the case of monodisperse polymers, it is well known that the phase behaviour depends strongly on the polymer-to-colloid diameter ratio (see e.g. [15, 21]). For small polymers only coexistence between colloidal fluid and solid phases is observed. (The term 'fluid' is used here because there are no distinguishable gas and liquid phases in such a system.) For larger polymers, on the other hand, with ξ above some threshold value ξ_c, a region of gas–liquid phase separation can occur in the phase diagram. When generalizing these considerations to the case of polydisperse polymers, there is no longer a single polymer size but rather a continuum of different diameters σ_p. A choice therefore needs to be made on how to define appropriately the typical polymer size that determines the phase behaviour. Ideally, one would like this definition to be such that phase diagrams become nearly independent of polymer polydispersity and can therefore be inferred from the corresponding monodisperse reference system [22].

A naive definition of the typical polymer size is the mean polymer diameter, $\xi_S = \int d\sigma_p\, \sigma_p n_p(\sigma_p)$. This is, in fact, independent of the diameter polydispersity δ, defined as the standard deviation of $n_p(\sigma_p)$ normalized by its mean. We will see below, however, that this provides a poor mapping from polydisperse to monodisperse systems, with phase behaviour at fixed ξ_S strongly dependent on δ. Following [22], we have therefore investigated other definitions of typical polymer size. These include the *number average* ξ_N, defined by

$$\xi_N^2 = \int d\sigma_p\, \sigma_p^2 n_p(\sigma_p). \tag{1}$$

This is proportional to the average polymer chain length, which scales as σ_p^2. The *mass average* ξ_M is also an average chain length, but with the contribution from each polymer size weighted by an additional factor of chain length (i.e. mass):

$$\xi_M^2 = \frac{\int d\sigma_p\, \sigma_p^4 n_p(\sigma_p)}{\int d\sigma_p\, \sigma_p^2 n_p(\sigma_p)}. \tag{2}$$

A final definition, the *virial average* ξ_B, is derived from the second virial coefficient for the polymer–colloid interaction. A polymer's centre of mass is excluded from a sphere of diameter $1+\sigma_p$ around a colloid of size $\sigma_c \equiv 1$, and ξ_B is defined as the monodisperse polymer diameter giving the same average excluded volume, namely

$$(1+\xi_B)^3 = \int d\sigma_p\, (1+\sigma_p)^3 n_p(\sigma_p). \tag{3}$$

In a monodisperse system all of these definitions are of course equivalent, so that $\xi_S = \xi_N = \xi_M = \xi_B$. In a polydisperse system they respond differently to the shape of the polymer diameter distribution, and we will try to identify which definition is best suited to characterizing the phase behaviour in a manner that depends only weakly on the polymer polydispersity. In assessing this dependence we also have a choice for an appropriate measure of polymer concentration. This could be e.g. the total polymer number density $\rho_p = \int d\sigma_p\, \rho_p(\sigma_p)$ or the effective volume fraction of the polymer spheres, $\phi_p = \int d\sigma_p\, \sigma_p^3 \rho_p(\sigma_p)$; values of ϕ_p of order unity correspond to the crossover from the dilute to the semi-dilute polymer regime. For a fixed diameter distribution $n_p(\sigma_p)$, ρ_p and ϕ_p are proportional to each other, but when comparing distributions with different shapes the difference in the proportionality coefficients matters. We choose mostly to work with ϕ_p, following Warren's suggestion [22] that this produces phase diagrams with a relatively weak dependence on the polymer diameter distribution. This will allow us to assess how far Warren's insight generalizes beyond the binary mixtures of small polymers which he considered.

As far as previous work on polymer polydispersity effects in colloid–polymer mixtures goes, we have already mentioned Warren's work for mixtures of polymers of two different sizes [22]. This explicitly accounted for the fact that the overall polymer density distribution in the system—which in the polydisperse case we will write as $\rho_p^{(0)}(\sigma_p)$—is imposed by the experimental conditions. Studies of polymers with continuous size polydispersity, on the other hand, have been restricted to the *semi-grand-canonical* case [23, 24]. (An exception is very recent work [25] on interacting polymers; see section 4.) Here the system is thought of as connected to a large polymer reservoir which fixes the chemical potential $\mu_p(\sigma_p)$ for each polymer size σ_p. The polymer density in the system is determined only indirectly, and has to be deduced *a posteriori*. Within the AO approach the polymers are treated as ideal so that the reservoir density distribution and chemical potentials are related by $\rho_p^r(\sigma_p) = e^{\mu_p(\sigma_p)}$. The decomposition of the chemical potential into ideal and excess parts, $\mu_p(\sigma_p) = \ln \rho_p(\sigma_p) + \mu_p^{ex}(\sigma_p)$, then shows that the polymer density distribution in any of the phases within the system itself can be written as

$$\rho_p(\sigma_p) = \rho_p^r(\sigma_p) e^{-\mu_p^{ex}(\sigma_p)}. \tag{4}$$

Here the $\mu_p^{ex}(\sigma_p)$ are the excess polymer chemical potentials of the phase being considered.

Figure 1 shows a sketch of the results obtained in [24] for such a semi-grand-canonical scenario, with polymer reservoir density distributions of Schulz form (see section 3 below). The graphs compare the behaviour for weak ($z \to \infty$, i.e. $\delta = 0$, dashed lines) and strong ($z = 5$, solid lines) polydispersity. The means of the Schulz distributions were chosen so that the virial average polymer size $\xi_B = 0.4$ of the normalized reservoir size distribution was the same in both cases. On the left, the polymer reservoir density ρ_p^r is sketched against the colloid

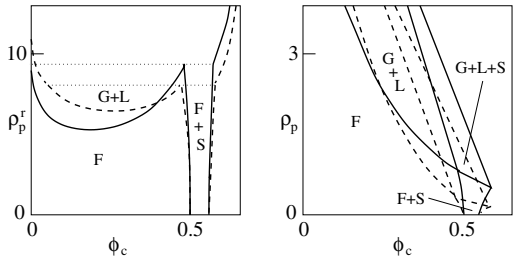

Figure 1. Phase diagram sketch of the phase behaviour for a semi-grand-canonical colloid–polymer mixture, following [24]; F: fluid, G: gas, L: liquid, S: solid. The two graphs show the colloid volume fraction on the horizontal axis and on the vertical axis the polymer reservoir density ρ_p^r (left) and the polymer density ρ_p in the system itself (right). The dashed and solid curves correspond to weak ($z \to \infty$, $\delta = 0$) and strong ($z = 5$) polymer polydispersity, respectively; the virial average polymer size is $\xi_B = 0.4$ in both cases. The triple points are marked by horizontal dotted lines on the left; they are mapped to three-phase GLS triangles on the right.

volume fraction. Using (4), these results can then be mapped onto a representation in terms of the actual polymer density ρ_p in the system, as shown on the right. This corresponds to fixing the total *number* of polymers in the system while the polymer *size distribution* continues to vary across the phase diagram, being controlled by the chemical potentials—or rather the chemical potential differences—imposed via the reservoir.

In both representations figure 1 shows that, as a general rule, increasing the polymer polydispersity δ increases the size of the gas–liquid region in the phase diagram. As seen most clearly in the plot on the right, however, there are also regions in the phase diagram (at low ρ_p) where gas–liquid coexistence is suppressed with increasing δ, and fluid–solid phase separation is favoured. This seems counter-intuitive: size polydispersity in the *colloids*, for example, is known to have the opposite effect, delaying fluid–solid relative to gas–liquid phase separation [21, 26, 27]. One of our aims will be to clarify this issue, and in particular the effect of the varying polymer size distribution in the semi-grand-canonical setting.

The effects of polymer size polydispersity have also been analysed in terms of the (pairwise part of the) depletion interaction between colloids [28–31]. Conceptually, the fixed polymer size distribution in these studies means again that constant imposed polymer chemical potentials are being considered; see e.g. [15, 32]. Finally, we mention the related work of [33]. This also used a semi-grand-canonical framework, but starting from a different physical motivation: polymers were regarded as monodisperse with regard to chain length, and size polydispersity in the equivalent polymer spheres was considered as arising from compression of the polymers. In this case the semi-grand-canonical approach is the physically relevant one since polymer spheres of different sizes can be transformed into each other. (A similar scenario arises when the polymers are replaced by wormlike micelles [34].) The effects of polymer compressibility on fluid–solid phase boundaries were found to be rather small up to size ratios $\xi \approx 0.5$ [33]. We therefore ignore them here and focus on size polydispersity arising from a distribution of polymer chain lengths. The experimental situation is then normally the canonical one, where the overall distribution of polymer sizes in the system is fixed.

Below we describe briefly the free energy which we use to model our colloid–polymer mixture, and the numerical method by which phase diagrams are obtained (section 2). Our results for the effects of polydispersity on the phase behaviour are given in section 3, separately for the experimentally relevant case of fixed polymer size distribution and for the semi-grand-canonical scenario where we compare with previous studies [24]. Conclusions and an outlook towards future work can be found in the final section.

2. Free energy and numerical method

In a recent paper [21] we derived a free-energy expression for an AO system where both polymers and colloids are polydisperse, by extending the free-volume approximation of Lekkerkerker *et al* [15]. This free energy can be written in the following form:

$$f = f_{\mathrm{c}}^{\mathrm{id}} + f_{\mathrm{p}}^{\mathrm{id}} + f_{\mathrm{hs}}^{\mathrm{ex}} + \int \mathrm{d}\sigma_{\mathrm{p}}\, \rho_{\mathrm{p}}(\sigma_{\mathrm{p}}) \mu_{\mathrm{hs}}^{\mathrm{ex}}(\sigma_{\mathrm{p}}). \tag{5}$$

The first two contributions are the ideal free energies of a mixture of polydisperse colloids and polymers, respectively. The next term, $f_{\mathrm{hs}}^{\mathrm{ex}}$, is the excess free energy of a system of pure (polydisperse) hard-sphere colloids. In the last term, which represents the colloid–polymer interaction, $\mu_{\mathrm{hs}}^{\mathrm{ex}}(\sigma_{\mathrm{p}})$ is the excess chemical potential of a hard-sphere particle of diameter σ_{p} in the pure colloid system.

Evaluation of the free energy (5) requires as input only the properties of the pure colloid system, i.e. its excess free energy $f_{\mathrm{hs}}^{\mathrm{ex}}$. We therefore need to assign appropriate expressions for $f_{\mathrm{hs}}^{\mathrm{ex}}$ in the colloidal fluid (or gas/liquid) and solid phases. For the *fluid* part of the excess free energy the most accurate approximation available is the BMCSL equation of state [35, 36] while for the *solid* we adopt Bartlett's fit to simulation data for bidisperse hard-sphere mixtures [37, 38]. Our previous work [26, 27] on polydisperse hard spheres has shown that with these free energy expressions quantitatively accurate fits to simulation data are obtained. Both free energy expressions depend only on the moments $\rho_{\mathrm{c}i} = \int \mathrm{d}\sigma_{\mathrm{c}}\, \rho_{\mathrm{c}}(\sigma_{\mathrm{c}}) \sigma_{\mathrm{c}}^{i}$ ($i = 0, \ldots, 3$) of the colloid density distribution. As a consequence the excess chemical potentials become third-order polynomials,

$$\mu_{\mathrm{hs}}^{\mathrm{ex}}(\sigma) = \frac{\delta f_{\mathrm{hs}}^{\mathrm{ex}}}{\delta \rho_{\mathrm{c}}(\sigma)} = \sum_{i} \mu_{\mathrm{hs},i}^{\mathrm{ex}} \sigma^{i} \tag{6}$$

where the $\mu_{\mathrm{hs},i}^{\mathrm{ex}}$ are the excess moment chemical potentials of the pure hard-sphere system, $\mu_{\mathrm{hs},i}^{\mathrm{ex}} = \partial f_{\mathrm{hs}}^{\mathrm{ex}} / \partial \rho_{\mathrm{c}i}$. (As explained in [21], we always evaluate these from the BMCSL free energy.) The interaction term in (5) then simplifies to

$$\int \mathrm{d}\sigma_{\mathrm{p}}\, \rho_{\mathrm{p}}(\sigma_{\mathrm{p}}) \mu_{\mathrm{hs}}^{\mathrm{ex}}(\sigma_{\mathrm{p}}) = \sum_{i} \mu_{\mathrm{hs},i}^{\mathrm{ex}} \rho_{\mathrm{p}i} \tag{7}$$

where the $\rho_{\mathrm{p}i} = \int \mathrm{d}\sigma_{\mathrm{p}}\, \rho_{\mathrm{p}}(\sigma_{\mathrm{p}}) \sigma_{\mathrm{p}}^{i}$ ($i = 0, \ldots, 3$) are the moments of the polymer density distribution.

We will deal with the particular case where the colloids are assumed to be monodisperse. With the colloid diameter set to unity as assumed, all colloid density moments then become identical, $\rho_{\mathrm{c}i} = \rho_{\mathrm{c}}$. Writing out the ideal contributions explicitly, the free energy (5) thus takes the form

$$f = \rho_{\mathrm{c}}(\ln \rho_{\mathrm{c}} - 1) + \int \mathrm{d}\sigma_{\mathrm{p}}\, \rho_{\mathrm{p}}(\sigma_{\mathrm{p}})[\ln \rho_{\mathrm{p}}(\sigma_{\mathrm{p}}) - 1] + f_{\mathrm{hs}}^{\mathrm{ex}}(\rho_{\mathrm{c}}) + \sum_{i} \mu_{\mathrm{hs},i}^{\mathrm{ex}}(\rho_{\mathrm{c}}) \rho_{\mathrm{p}i}. \tag{8}$$

Here we have highlighted that $f_{\mathrm{hs}}^{\mathrm{ex}}$ (and therefore the $\mu_{\mathrm{hs},i}^{\mathrm{ex}}$) now only depend on the colloid density ρ_{c}, or equivalently the colloidal volume fraction ϕ_{c}; for monodisperse colloids and in our units the two quantities are identical. The excess part of the free energy (8) thus only depends on the colloid density ρ_{c} and the moments $\rho_{\mathrm{p}i}$ of the polymer density distribution. As in [21] for the converse situation of polydisperse colloids and monodisperse polymers, we can regard these quantities as moments of an enlarged density distribution (ρ_{c}, $\rho_{\mathrm{p}}(\sigma_{\mathrm{p}})$). Because only a finite number (five) of such moments are involved, we thus have a *truncatable* free energy [39]. The phase equilibrium conditions associated with this free energy can then be solved using the moment-free-energy (MFE) method [21, 39–42]. The moment free energy

allows one to map the full free energy (8), with its dependence on all details of $\rho_p(\sigma_p)$ through the ideal part, onto an MFE depending only on the moments ρ_{pi} and ρ_c. From the latter, phase behaviour can then be found by the conventional methods for finite mixtures, treating each of the ρ_{pi} as a number density of an appropriate 'quasi-species' [39]. For truncatable free energies this locates exactly the cloud points, i.e. the onset of phase separation coming from a single phase, as well as the properties of the coexisting 'shadow' phases that appear. Inside the coexistence region, one in principle needs to solve a set of highly coupled nonlinear equations, and the predictions derived from the MFE are only approximate. However, by retaining extra moments, increasingly accurate solutions can be obtained by iteration [39, 43–45]. Using these as initial points, we are then able to find the, for our free energy, exact solutions of the phase equilibrium equations.

The MFE method is designed for the physically realistic scenario where the overall polymer density distribution is conserved when the system separates into two or more phases. However, it can also be exploited to analyse semi-grand-canonical settings. This is done by relaxing the particle conservation constraints on some moments; in our specific case, only ρ_c and ρ_{p0} are kept conserved while the other moments of the polymer density distribution are adapted to minimize the free energy. One can show that this reproduces the semi-grand-canonical analysis of Sear and Frenkel [24], in full analogy to our discussion in [27].

3. Phase behaviour

In this section we will describe our results for the overall phase behaviour of a mixture of polydisperse polymers and monodisperse hard-sphere colloids. Our numerical work requires a choice to be made for the 'parent' polymer diameter distribution $n_p^{(0)}(\sigma_p)$ which is imposed when the system is prepared. We concentrate primarily on a Schulz distribution

$$n_p^{(0)}(\sigma_p) \propto \sigma_p^z \exp\left[-\left(\frac{z+1}{\bar{\sigma}}\right)\sigma_p\right].$$

An upper cut-off of $\sigma_p = 1$ on polymer sizes is imposed because for larger sizes the chain structure of the polymers becomes important and polymers can no longer be treated as effective spheres; see e.g. [46, 47]. The parameters $\bar{\sigma}$ and z control the mean and width of the Schulz distribution. Without a cut-off, the mean size is simply $\xi_S = \bar{\sigma}$ while the polydispersity is related to z via $\delta^2 = 1/(z+1)$. In the presence of the cut-off these relations remain valid for large z, where the system is almost monodisperse; otherwise z and $\bar{\sigma}$ have to be calculated numerically to give the desired values of ξ_S and δ. We will focus in our numerical work on three values of the polydispersity, namely $\delta = 1/\sqrt{20+1} \approx 0.22$, $\delta = 1/\sqrt{5+1} \approx 0.41$ and $\delta = 1/\sqrt{2+1} \approx 0.58$.

To check the generality of our results, calculations have also been performed for a triangular size distribution:

$$n_p^{(0)}(\sigma_p) = \frac{1}{w^2}\begin{cases} \sigma_p - (\bar{\sigma} - w) & \text{for } \bar{\sigma} - w \leqslant \sigma_p \leqslant \bar{\sigma} \\ (\bar{\sigma} + w) - \sigma_p & \text{for } \bar{\sigma} \leqslant \sigma_p \leqslant \bar{\sigma} + w \end{cases}.$$

Here the mean size is $\xi_S \equiv \bar{\sigma}$ independently of the width parameter w, which is related to the polydispersity by $w = \sqrt{6}\bar{\sigma}\delta$. We find that qualitative features do not depend strongly on the shape of the polymer size distribution and so mostly report only the results for a Schulz distribution.

3.1. Phase diagrams

As discussed in the introduction, the phase diagrams of monodisperse colloid–polymer mixtures may show either only fluid–solid coexistence or, for sufficiently large polymers,

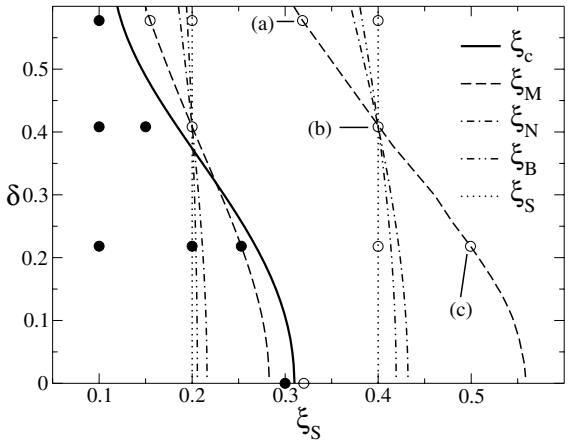

Figure 2. Phase diagram topologies as a function of mean polymer size ξ_S and polydispersity δ. Full circles indicate parameter values where only fluid–solid coexistence is found, while empty circles show that the phase diagram has a gas–liquid coexistence region. The thick solid curve shows a rough estimate for the boundary between the two regions, which defines the crossover value of the mean polymer size, $\xi_c(\delta)$. Two sample sets of curves corresponding to constant ξ_S, ξ_N, ξ_M and ξ_B (chosen to agree at $\delta = 0.41$) are also drawn. Comparison with the thick solid curve shows that ξ_M is most suitable for predicting the phase diagram topology independently of δ.

an additional gas–liquid region with an associated gas–liquid–solid triangle. We begin by investigating the effect of polymer polydispersity on the change in phase diagram topology as polymer size is increased, by calculating phase diagrams for a range of values of mean polymer size ξ_S and polymer polydispersity δ. Figure 2 summarizes the results, for Schulz size distributions. The empty circles indicate phase diagrams containing gas–liquid coexistence regions, while the full circles identify phase diagrams where only a fluid to fluid–solid transition was found. From these results we can estimate the threshold value ξ_c for the mean polymer diameter as a function of polydispersity δ, as indicated by the thick solid curve in figure 2. The data show that as polydispersity increases, ξ_c diminishes significantly. This is due to the fact that, for given ξ_S, polydispersity tends to favour gas–liquid over fluid–solid coexistence. At $\xi_S = 0.2$, for example, the phase diagram topology changes at $\delta \approx 0.35$, from fluid–solid coexistence only at low δ to additional gas–liquid and gas–liquid–solid coexistence at high δ.

In figure 3 we show the full phase diagram obtained for Schulz distributions of polydispersity $\delta = 0.41$ and 0.58 and at constant mean polymer size of $\xi_S = 0.2$ (top) and $\xi_S = 0.4$ (bottom). The axis variables are the colloid volume fraction ϕ_c—identical in our units to ρ_c—and the (effective) polymer volume fraction $\phi_p = \rho_{p3}$, following the suggestion by Warren [22] that the representation in terms of ϕ_p minimizes polydispersity effects on the phase behaviour. At $\xi_S = 0.2$ we see explicitly how gas–liquid and three-phase regions appear as δ is increased, while the fluid–solid boundary recedes. At $\xi = 0.4$, figure 3 (bottom), a gas–liquid region is present for all polydispersities. The main effect of increasing polydispersity is again to favour gas–liquid coexistence. We note that, in contrast to what is found in a monodisperse system, the phase boundaries of the gas–liquid–solid region are no longer straight. This is due to the fact that in a polydisperse system the constraint of particle conservation must be satisfied for infinitely many different polymer sizes; indeed, the polymer size distributions of the three coexisting phases change as one moves around the three-phase region.

We next ask which measure of effective polymer size is most appropriate for predicting the phase diagram topology. Ideally, as explained in the introduction, the value of this quantity

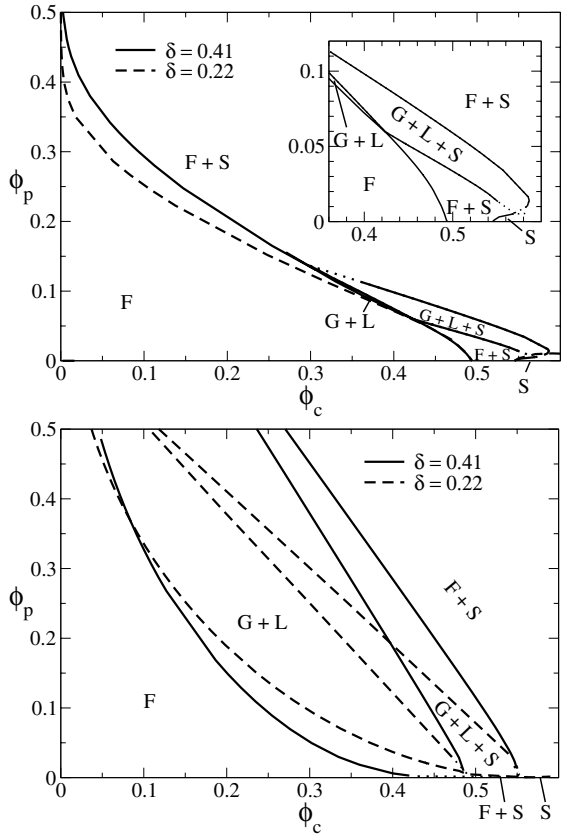

Figure 3. Phase diagrams for Schulz distributions with polydispersity $\delta = 0.41$ and 0.58 and fixed mean polymer size $\xi_S = 0.2$ (top) and $\xi_S = 0.4$ (bottom), plotted in terms of effective polymer volume fraction ϕ_p versus colloid volume fraction ϕ_c. Dotted curve: best guess for the phase boundary where our numerical data become unreliable. The inset shows an enlarged view of the three-phase region for $\delta = 0.41$ and $\xi_S = 0.2$.

should be enough to predict the occurrence or not of gas–liquid coexistence, whatever the polydispersity. In terms of figure 2, this means that the curve $\xi_c(\delta)$ should follow a contour of constant effective polymer size. We have therefore plotted such contours for each of the four possible measures of effective size discussed in the introduction (ξ_S, mean diameter; ξ_N, number average; ξ_M, mass average; ξ_B, virial average). Two sets of contours are shown, chosen such that all four quantities have identical values (0.2 and 0.4, respectively) at polydispersity $\delta = 1/\sqrt{5+1} \approx 0.41$. This value of δ was also used as a reference point in [24]. We see that among the four candidate definitions of an effective polymer size, the mass average gives a contour which follows most closely—although certainly not perfectly—the curve $\xi_c(\delta)$ which marks the crossover between the two phase diagram topologies. It is therefore our best candidate for a useful measure of effective polymer size.

We can now go further and investigate whether polymer size distributions with the same mass-average ξ_M have not only the same phase diagram topology but in fact *quantitatively* similar phase diagrams. As pointed out in the introduction, the answer to this question also depends on how we represent the concentration of polymers; we continue to use ϕ_p. With this choice, the collapse of phase diagrams for polymer size distributions with the same ξ_M

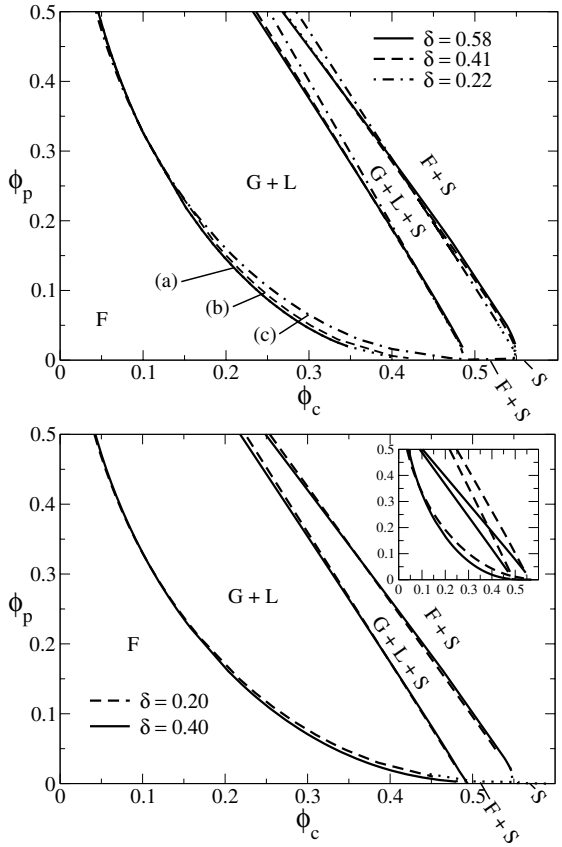

Figure 4. Top: phase diagrams for Schulz distributions with polydispersity $\delta = 0.22$, 0.41 and 0.58 and constant mass average $\xi_M = 0.558$; this should be contrasted with figure 3, where the mean size ξ_S (=0.4) was held fixed. Bottom: phase diagrams for a triangular size distribution with $\delta = 0.2$ and 0.4 at constant mass average $\xi_M = 0.528$. In the inset the results for fixed mean diameter of $\xi_S = 0.4$ are shown for comparison. Dotted curves indicate best guesses for phase boundaries we could not determine accurately from our numerics.

is in fact rather good, as shown in figure 4 (top). The phase diagrams displayed correspond to the parameter values at points (a)–(c) in figure 2. In figure 4 (bottom) we show analogous results for triangular size distributions. Again the comparison at constant mass-average ξ_M gives a good collapse of the phase diagrams for different polydispersities, while at fixed ξ_S polydispersity causes significant changes; see the inset of figure 4 (bottom). In summary, we can say that systems with the same mass-average ξ_M give phase diagrams which are not only qualitatively but in fact quantitatively largely independent of polydispersity. Our results suggest that this conclusion holds independently of the polymer size distribution—though multimodal distributions might be expected to behave differently—and up to fairly substantial polydispersities of at least 40% and possibly higher.

We note finally that the results in figure 4 are for the case of relatively large polymers, where phase separation is initially into gas and liquid except at very low polymer concentrations. We have checked the near δ-independence of phase diagrams with the same ξ_M also for smaller polymers, where fluid–solid phase separation occurs first (data not shown), and reached the same conclusion. Very close to the crossover in the phase diagram topology, deviations do of

course appear. This is clear from figure 2, which shows that the contour of constant ξ_M does not follow the crossover curve perfectly. In a narrow range of fixed values of ξ_M the phase diagram will therefore change with δ, both in terms of its topology and the quantitative location of the phase boundaries.

3.2. Comparison with semi-grand-canonical approach

The qualitative trend of the results presented so far is that, for fixed mean polymer size ξ_S, polymer polydispersity favours gas–liquid coexistence over fluid–solid phase splits. On the other hand, the results obtained by Sear and Frenkel in the semi-grand-canonical approach [24], as sketched in figure 1, suggested that fluid–solid phase separation can be favoured by polydispersity in some regions of the phase diagram. This difference clearly needs to be understood.

Three possible causes suggest themselves. First, the results of Sear and Frenkel were obtained by comparing reservoir polymer size distributions with constant virial average size ξ_B, whereas we initially focused on constant ξ_S. Second, their phase diagrams are represented in terms of polymer density ρ_p rather than effective polymer volume fraction ϕ_p. Third, their polymer size distribution in the system varies because it is imposed only indirectly via the reservoir size distribution, whereas it is fixed in our analysis.

It is intuitively clear from the discussion above that keeping ξ_B rather than ξ_S constant should not influence the results greatly. Indeed, if we look at figure 2 we see that contours of constant ξ_B are close to those for constant ξ_S, which are vertical lines. To rule out more quantitatively the first two possible reasons discussed above, we have calculated the cloud curves for the onset of gas–liquid coexistence for three Schulz size distributions with identical ξ_B, and plotted them in figure 5 (top) with ρ_p on the vertical axis. As before, gas–liquid coexistence is favoured by increased polymer polydispersity. This leaves only the third reason, i.e. the difference between the canonical and semi-grand-canonical scenarios. Figure 5 (bottom) compares our results for the semi-grand-canonical scenario with the canonical ones in the top graph. The same three polymer size distributions are used as before, but they now specify the properties of the reservoir: the normalized reservoir size distribution, $n_p^r(\sigma_p)$, is the same as the parent size distribution $n_p^{(0)}(\sigma_p)$ used in the canonical case. As expected, our semi-grand-canonical results are in good agreement[1] with those of [24]. In particular, we see in figure 5 (bottom) that the change to the semi-grand-canonical description has *reversed* the order of the cloud curves at low polymer density as compared to the canonical scenario shown in figure 5 (top).

We can thus conclude that the opposite trends with polydispersity seen in the present study and in [24] arise from the choice of a semi-grand-canonical scenario in the latter. To understand explicitly how the polymer size distribution is affected by this, we can combine (4) and (6) to write

$$\rho_p(\sigma_p) = \rho_p^r(\sigma_p) \exp\left(- \sum_{i=0}^{3} \mu_{hs,i}^{ex} \sigma_p^i \right) \tag{9}$$

where $\rho_p^r(\sigma_p)$ is the polymer density distribution in the reservoir as before. The excess chemical potentials $\mu_{hs,i}^{ex}$ that appear here vary as we change the colloid density of our system. Correspondingly the polymer density distribution has its shape modified as we move around the phase diagram. In particular, at the onset of phase coexistence the normalized size distribution

[1] It appears that figure 4 in [24] may have been incorrectly scaled: on the horizontal axis, which represents a pure hard-sphere colloid system without polymer, the onset of fluid–solid coexistence is shown at $\phi_c \approx 0.525$ rather than the correct value $\phi_c = 0.494$ which our calculation and the other figures in [24] reproduce.

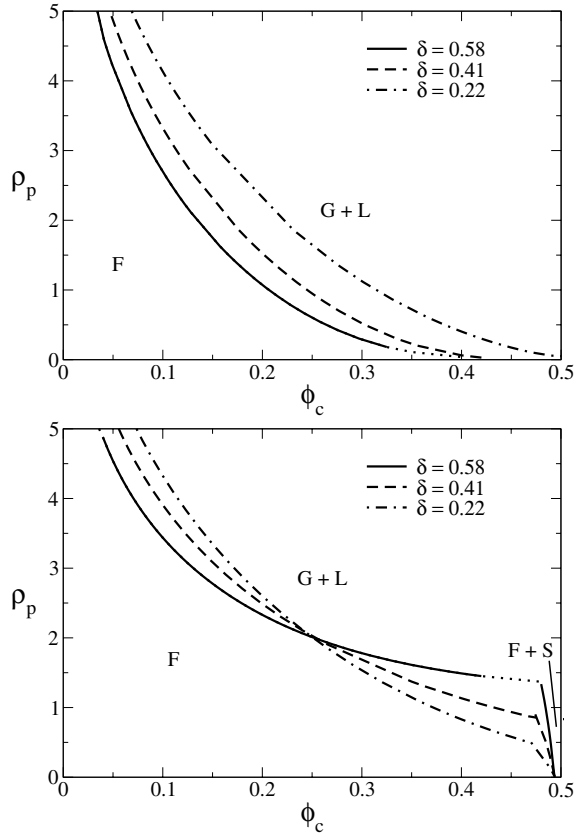

Figure 5. Cloud curves showing the onset of phase coexistence coming from low colloid density. Top: canonical scenario; results are shown for three parent size distributions $n_{\rm p}^{(0)}(\sigma_{\rm p})$ with different polydispersities, all with the same virial average polymer size $\xi_{\rm B}$ as the reference distribution with $\xi_{\rm S} = 0.4$ and $\delta = 0.41$. Bottom: results for the corresponding semi-grand-canonical scenario, where the same three distributions are used as the *reservoir* size distribution, $n_{\rm p}^{\rm r}(\sigma_{\rm p})$.

$n_{\rm p}(\sigma_{\rm p})$ will differ from the one in the reservoir, $n_{\rm p}^{\rm r}(\sigma_{\rm p})$. In the more realistic canonical description, on the other hand, $n_{\rm p}(\sigma_{\rm p}) = n_{\rm p}^{(0)}(\sigma_{\rm p})$ remains fixed up to the point where phase coexistence begins.

To illustrate this difference, we plot in figure 6 (top) the normalized size distributions $n_{\rm p}(\sigma_{\rm p})$ in the semi-grand-canonical system (solid curves). These are compared to the reservoir size distributions $n_{\rm p}^{\rm r}(\sigma_{\rm p})$ (dashed curves), which are the same as used in figure 5 (bottom); the colloid and polymer densities are $(\phi_{\rm c}, \rho_{\rm p}) = (0.3, 1.0)$. We notice that the system and reservoir size distributions differ significantly: the Gibbs–Boltzmann factor in (9) shifts the mean polymer size to lower values, and this effect becomes stronger as the polydispersity increases. Figure 6 (bottom) traces the mean and polydispersity of the system size distribution as a function of colloid volume fraction $\phi_{\rm c}$, at fixed $\rho_{\rm p} = 1.0$. The reduction in the mean size compared to the reservoir is seen to increase with colloid density. The polydispersity, on the other hand, is only weakly affected, as the inset of figure 6 (bottom) shows.

The lines in figure 6 (bottom) are drawn up to the cloud point where phase separation begins. For the widest reservoir distribution ($\delta = 0.58$), the mean polymer size in the system

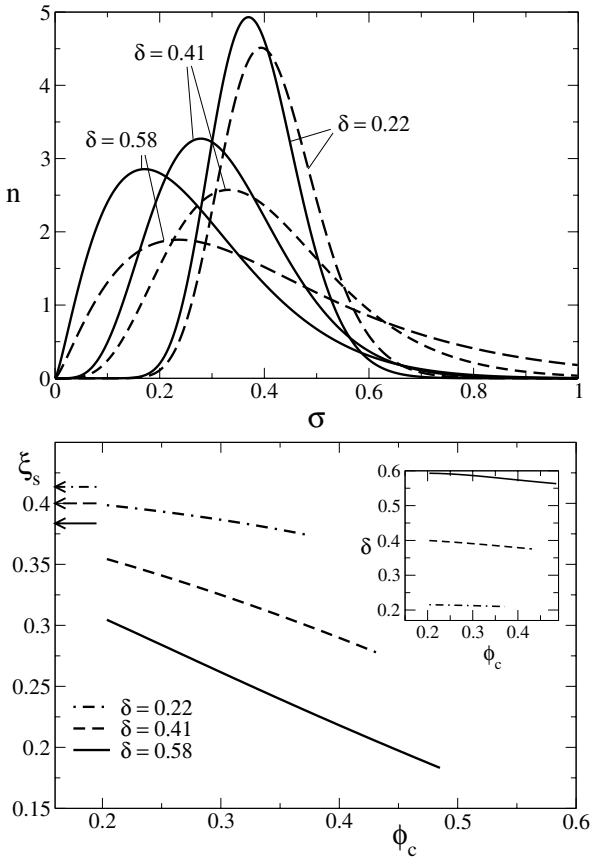

Figure 6. Top: comparison of polymer size distributions in a semi-grand-canonical system, $n_p(\sigma_p)$ (solid lines), with the corresponding reservoir size distributions $n_p^r(\sigma_p)$ (dashed). The same three reservoir distributions as in figure 5 (bottom) are used; the colloid and polymer densities are fixed to $(\phi_c, \rho_p) = (0.3, 1.0)$. Bottom: mean polymer size ξ_S (main graph) and polydispersity δ (inset) of the system size distribution $n_p(\sigma_p)$, at fixed polymer density $\rho_p = 1.0$ and for varying colloid density ϕ_c. Arrows on the vertical axis in the main plot indicate the mean sizes in the reservoir.

at this point is roughly half that in the reservoir. Because smaller polymers produce a depletion interaction that is both weaker and more short ranged, this reduction in polymer size delays the onset of phase separation. Overall, we conclude that the inversion in the order of the cloud curves in the bottom part of figure 5 (bottom) results from the shift of the polymer size distribution to lower values as the polydispersity of the reservoir is increased.

The reduction of the polymer mean size in the semi-grand-canonical scenario can be understood quantitatively for narrow reservoir distributions. Looking at (9), if $\rho_p^r(\sigma_p)$ is narrowly peaked around $\sigma_p = \xi_S^r$, then we can expand the exponential as const$\times[1-\lambda(\sigma_p-\xi_S^r)]$ to leading order. From this one easily sees that the mean size ξ_S in the system is

$$\xi_S = \xi_S^r - \lambda\langle(\sigma_p - \xi_S^r)^2\rangle_r = \xi_S^r - \lambda\delta^2(\xi_S^r)^2 \tag{10}$$

to lowest order in δ. The coefficient λ must be positive because the excess chemical potential in a hard-sphere system, $\mu_{hs}^{ex}(\sigma_p)$, is an increasing function of σ_p. As expected we have, therefore, a reduction in the mean polymer size compared to the reservoir, by an amount which grows with the reservoir polydispersity as δ^2.

Finally, we note that the three curves in figure 5 (bottom) all appear to cross at the same point. To see how this effect arises, we focus again on narrow reservoir distributions. The location of the cloud point value of the polymer density $\rho_p = \rho_p(\phi_c, \xi_S, \delta)$ depends on the colloid volume fraction ϕ_c, the mean polymer size ξ_S in the system and the polydispersity δ; for small δ, other properties of the size distribution are irrelevant. In a semi-grand-canonical setting, ξ_S and δ are determined indirectly by the colloid volume fraction ϕ_c as well as the mean polymer size ξ_S^r and the polydispersity of the reservoir. In a perturbation expansion to order δ^2 we can approximate δ^2 by its fixed value in the reservoir, and write $\xi_S = \xi_S^r - \lambda\delta^2(\xi_S^r)^2$ from (10). The explicit dependence on δ of the cloud point is also expected to be quadratic to leading order [48, 49]. Overall, we can therefore expand the cloud point position in a weakly polydisperse semi-grand-canonical system as

$$\rho_p(\phi_c, \xi_S, \delta) = \rho_p(\phi_c, \xi_S^r, 0) - \lambda\delta^2(\xi_S^r)^2\frac{\partial\rho_p}{\partial\xi_S}(\phi_c, \xi_S^r, 0) + \delta^2\frac{\partial\rho_p}{\partial\delta^2}(\phi_c, \xi_S^r, 0). \tag{11}$$

How this varies with increasing polydispersity δ^2 depends on the competition of the last two terms. The last term is also present in the canonical scenario and represents the shift in the cloud point at constant mean polymer size. We saw above that polydispersity favours phase coexistence under these conditions, so that $\partial\rho_p/\partial\delta^2$ must be negative; see also figure 5 (top). The second term is only present for the semi-grand-canonical case; because increasing ξ_S again favours phase separation, we have that also $\partial\rho_p/\partial\xi_S$ is negative. Thus the two δ^2-terms in (11) have opposite signs. The coefficient λ depends on ϕ_c; it tends to zero for $\phi_c \to 0$, where the excess chemical potentials in a hard-sphere system vanish, and grows from there with increasing ϕ_c. At small ϕ_c we therefore expect the third term in (11) to dominate, so that polydispersity favours phase separation as in the canonical case. As ϕ_c increases, the second term eventually balances the third. At this point the cloud curve is unaffected by δ^2 to leading order, and this produces the crossing phenomenon in figure 5 (bottom). At even higher ϕ_c, the second term dominates and so phase separation is delayed with increasing δ, exactly as seen in the lower part of figure 5 (bottom).

Overall, while in the realistic canonical description polydispersity always favours gas–liquid phase separation, in the semi-grand-canonical scenario this trend can be counteracted by a decrease in the mean polymer size in the system. This effect can become dominant at high colloid volume fractions, producing the reversal in the order of the curves in the lower parts of figure 5 (top) and (bottom).

4. Conclusion and outlook

We have investigated the effect of polymer polydispersity on a mixture of ideal polymers and hard-sphere colloids. Our focus was on the realistic (canonical) case where the distribution of polymer sizes is fixed when the system is prepared, but we have also compared with semi-grand-canonical approaches where the size distribution adapts by equilibrating to chemical potentials imposed by a large polymer reservoir [24]. For the canonical setting, gas–liquid phase separation is favoured by increased polydispersity while fluid–solid phase separation is retarded. This is in broad agreement with the intuition that polydispersity disfavours ordered phases [21, 27], though less obvious here since the size polydispersity is in the polymers, not in the colloids that order translationally in the solid.

In a semi-grand-canonical scenario the above trends with polydispersity are reversed in some parts of the phase diagram [24]. We saw that this arises because the polymer size distribution in the system can become rather different from the reservoir size distribution, especially for dense colloidal phases. Specifically, the size distribution is shifted to smaller

polymer sizes, the more so the larger the degree of polydispersity. This effect is sufficiently strong to reverse the order of the cloud curves compared to the canonical setting, favouring fluid–solid over gas–liquid formation.

For the canonical case of conserved polymer size distribution, we established that the phase diagram topology was nearly independent of polydispersity provided one compares systems with the same mass average polymer size ξ_M. We were led to this observation by estimating the location of the curve $\xi_c(\delta)$ in the (ξ_S, δ) plane along which the phase diagram topology changes, and comparing this with contours of constant ξ_M. The crossover value ξ_c decreases with increasing polydispersity δ, showing quantitatively that gas–liquid coexistence is favoured as polydispersity is increased at constant mean polymer size. Finally, we showed that even quantitatively the phase diagrams of systems with the same mass average ξ_M are nearly independent of polydispersity, provided that polymer concentration is represented in terms of the effective polymer volume fraction ϕ_p.

To assess the reliability of our results, we discuss briefly the approximations made. We have employed the standard AO model instead of explicitly modelling ideal polymer chains. Simulations [11] suggest that this is a reasonable approximation for polymers which are not too large, i.e. $\sigma_p < 1$. A slight improvement can be obtained by using a mapping from polymer radius of gyration to effective sphere radius $\sigma_p/2$ which accounts for the effect of the curvature of the colloid surface on the polymer conformations [11, 50]. In the limit of a small polymer, this results in an increase of σ_p by a factor $2/\sqrt{\pi} \approx 1.13$ over the naive value, but in the range $0.2 < \sigma_p < 1$ of interest the corrections to σ_p are small (<5%). With such corrections included, a Schulz distribution across the polymers' radii of gyration—the case we concentrated on—would result in a distribution of σ_p that is no longer precisely of Schulz form; quantitatively, however, this will again be a small effect. We have also used the free-volume approximation to estimate the free energy of the polydisperse AO model. As discussed elsewhere [21], this is essentially equivalent to the density functional theory approach of [33]; see also the discussion for the monodisperse case in [17]. Again, simulations suggest that this approach is reliable [11, 20] in the range $0.3 < \sigma_p < 1$, although somewhat less so after polymer reservoir densities ρ_p^r are converted back to those in the system (compare e.g. figure 3 in [20] with figure 2(b) in [17]).

We comment briefly on comparisons with experimental work. Much work on mixtures of colloids and θ-point polymers has been done in Edinburgh; see e.g. the review [34]. Experimentally, the typical polymer size is normally determined from the weight-average molecular weight, which corresponds to our ξ_M^2. Interestingly, our results then suggest that polymer polydispersity should have only a small effect on the phase behaviour, so that e.g. the comparison between experimental data and AO model predictions in [51] would remain essentially unchanged[2]. A systematic experimental study of such polydispersity effects would seem worthwhile. For example, one could prepare two polydisperse systems, one whose number-averaged molecular weight ($\sim\xi_N^2$) and one whose mass-averaged molecular weight ($\sim\xi_M^2$) coincides with that of a near-monodisperse reference system; our theory would then predict that the second polydisperse system produces phase behaviour much more similar to the monodisperse reference than the first. Also fruitful could be the investigation of polymer size

[2] However, care is needed when comparing measures of polymer concentrations. Whereas we have used the effective polymer volume fraction ϕ_p, experimentally the polymer mass density is more readily accessible; in our units, the latter is proportional to $\rho_p\xi_N^2$. At constant ξ_M, one finds e.g. for a Schulz distribution that the ratio $\phi_p/(\rho_p\xi_N^2) = \langle\sigma_p^3\rangle/\langle\sigma_p^2\rangle$ *decreases* with increasing polymer polydispersity δ. Since we found phase diagrams that were relatively insensitive to δ when expressed in terms of ϕ_p, the corresponding values of polymer mass density should *increase* with δ. Quantitatively the effect is moderate, however, leading to an increase of only ≈10% over the monodisperse case even for $\delta = 0.6$.

fractionation between coexisting phases. We have not displayed our theoretical predictions for this; one finds as in the semi-grand-canonical approach [24] that the larger polymers are found in the phases with lower colloid density, but the detailed distribution shapes are different because they always need to combine to give the fixed parent distribution.

An interesting extension of the present work would be to consider the combined effect of polymer *and* colloid size polydispersity, generalizing the present study and our previous one on polydisperse colloids and monodisperse polymers [21]. This is in principle possible using the current framework, but the excess free energy would then depend on eight moments ρ_{ci} and ρ_{pi} ($i = 0, \ldots, 3$), making the problem very challenging numerically. Physically, one would expect from our current results that the crossover value of the polymer size, when measured in terms of the mass average ξ_M, would be largely unaffected by *polymer* polydispersity, but decrease significantly with increasing *colloid* polydispersity [21]. A simpler alternative to the treatment of a fully polydisperse system would be to consider the colloid size distribution as 'quenched', i.e. equal to the parent in all phases, thus excluding colloid size fractionation. One would then need only one conserved colloid moment in the excess free energy, and the complexity of the numerical analysis would be the same as in the present study. Physically, this quenched approximation could be appropriate for describing the initial stages of phase separation in a polydisperse colloid–polymer mixture, where *polymer* size fractionation—which should be the faster process—has already taken place while *colloid* size fractionation is still negligible.

A key open question for further work is how our results generalize to the case of good or poor (rather than θ-) solvents, where polymer–polymer interactions can no longer be neglected. For monodisperse polymers this issue has been tackled by a variety of methods including virial expansions near the θ-point [52], integral equations [53–56], Flory–Huggins theory [57], coarse-graining of polymers into soft colloids [20, 50, 58], modifications of free-volume theory [59], and an AO model with added soft polymer–polymer repulsions [60] to model good solvents or with a repulsive co-solvent to mimic poor ones [61]. It remains an open challenge to incorporate polymer polydispersity into these approaches. Some progress in this direction has already been made in [25], which was published after the present work was completed. In this study the polymers were modelled as chains of hard-sphere particles, as would be appropriate for good solvent conditions, and calculations for the onset of gas–liquid coexistence were performed using a truncatable model free energy derived from thermodynamic perturbation theory [62]. Also in this scenario with interacting polymers, it is found that polydispersity significantly enlarges the size of the coexistence region. It appears therefore that this qualitative conclusion is robust to the presence or otherwise of polymer non-ideality. If the approach of [25] can be extended to include colloidal solids, it would be interesting to ask whether polydispersity effects on the relative stability of fluid–solid and gas–liquid phase separation are likewise robust under the inclusion of polymer–polymer interactions.

Acknowledgments

The authors acknowledge support of the EPSRC through grant number GR/R52121/01.

References

[1] Vincent B 1974 *Adv. Colloid Interface Sci.* **4** 193
[2] Napper D 1983 *Polymeric Stabilization of Colloidal Dispersions* (New York: Academic)
[3] Russel W B, Saville D A and Schowalter W R 1989 *Colloidal Dispersions* (Cambridge: Cambridge University Press)
[4] Enikolopyan N S, Fridman M L, Stalnova I O and Popov V L 1990 *Adv. Polym. Sci.* **96** 1
[5] Lewis J A 2000 *J. Am. Ceram. Soc.* **83** 2341

[6] Asakura S and Oosawa F 1954 *J. Chem. Phys.* **22** 1255
[7] Asakura S and Oosawa F 1958 *J. Polym. Sci.* **33** 183
[8] Vrij A 1976 *Pure Appl. Chem.* **48** 471
[9] Joanny J F, Leibler L and de Gennes P G 1979 *J. Polym. Sci.* B **17** 1073
[10] Meijer E J and Frenkel D 1991 *Phys. Rev. Lett.* **67** 1110
[11] Meijer E J and Frenkel D 1994 *J. Chem. Phys.* **100** 6873
[12] Gast A P, Hall C K and Russel W B 1983 *J. Colloid Interface Sci.* **96** 251
[13] Vincent B 1987 *Colloids Surf.* **24** 269
[14] Vincent B, Edwards J, Emmett S and Croot R 1988 *Colloids Surf.* **31** 267
[15] Lekkerkerker H N W *et al* 1992 *Europhys. Lett.* **20** 559
[16] Schmidt M, Löwen H, Brader J M and Evans R 2000 *Phys. Rev. Lett.* **85** 1934
[17] Schmidt M, Löwen H, Brader J N and Evans R 2002 *J. Phys.: Condens. Matter* **14** 9353
[18] Brader J M, Evans R and Schmidt M 2003 *Mol. Phys.* **101** 3349
[19] Dijkstra M, Brader J M and Evans R 1999 *J. Phys.: Condens. Matter* **11** 10079
[20] Bolhuis P G, Louis A A and Hansen J P 2002 *Phys. Rev. Lett.* **89** 128302
[21] Fasolo M and Sollich P 2004 *J. Chem. Phys.* at press
(Fasolo M and Sollich P 2004 *Preprint* cond-mat/0410374)
[22] Warren P B 1997 *Langmuir* **13** 4588
[23] Lee J T and Robert M 1999 *Phys. Rev.* E **60** 7198
[24] Sear R P and Frenkel D 1997 *Phys. Rev.* E **55** 1677
[25] Paricaud P, Varga S, Cummings P T and Jackson G 2004 *Chem. Phys. Lett.* **398** 489
[26] Fasolo M and Sollich P 2003 *Phys. Rev. Lett.* **91** 068301
[27] Fasolo M and Sollich P 2004 *Phys. Rev.* E **70** 041410
[28] Walz J Y 1996 *J. Colloid Interface Sci.* **178** 505
[29] Piech M and Walz J Y 2000 *J. Colloid Interface Sci.* **225** 134
[30] Goulding D and Hansen J P 2001 *Mol. Phys.* **99** 865
[31] Tuinier R and Petukhov A V 2002 *Macromol. Theory Simul.* **11** 975
[32] Dijkstra M and van Roij R 1997 *Phys. Rev.* E **56** 5594
[33] Denton A R and Schmidt M 2002 *J. Phys.: Condens. Matter* **14** 12051
[34] Poon W C K 2002 *J. Phys.: Condens. Matter* **14** R859
[35] Boublik T 1970 *J. Chem. Phys.* **53** 471
[36] Mansoori G A, Carnahan N F, Starling K E and Leland T W Jr 1971 *J. Chem. Phys.* **54** 1523
[37] Bartlett P 1999 *Mol. Phys.* **97** 685
[38] Bartlett P 1997 *J. Chem. Phys.* **107** 188
[39] Sollich P, Warren P B and Cates M E 2001 *Adv. Chem. Phys.* **116** 265
[40] Sollich P and Cates M E 1998 *Phys. Rev. Lett.* **80** 1365
[41] Warren P B 1998 *Phys. Rev. Lett.* **80** 1369
[42] Sollich P 2002 *J. Phys.: Condens. Matter* **14** R79
[43] Clarke N *et al* 2000 *J. Chem. Phys.* **113** 5817
[44] Speranza A and Sollich P 2002 *J. Chem. Phys.* **117** 5421
[45] Speranza A and Sollich P 2003 *J. Chem. Phys.* **118** 5213
[46] Sear R P 2001 *Phys. Rev. Lett.* **86** 4696
[47] Schmidt M and Fuchs M 2002 *J. Chem. Phys.* **117** 6308
[48] Evans R M L, Fairhurst D J and Poon W C K 1998 *Phys. Rev. Lett.* **81** 1326
[49] Evans R M L 2001 *J. Chem. Phys.* **114** 1915
[50] Louis A A, Bolhuis P G, Meijer E J and Hansen J P 2002 *J. Chem. Phys.* **117** 1893
[51] Ilett S M, Orrock A, Poon W C K and Pusey P N 1995 *Phys. Rev.* E **51** 1344
[52] Warren P B, Ilett S M and Poon W C K 1995 *Phys. Rev.* E **52** 5205
[53] Fuchs M and Schweizer K S 2000 *Europhys. Lett.* **51** 621
[54] Fuchs M and Schweizer K S 2001 *Phys. Rev.* E **64** 021514
[55] Fuchs M and Schweizer K S 2002 *J. Phys.: Condens. Matter* **14** R239
[56] Ramakrishnan S, Fuchs M, Schweizer K S and Zukoski C F 2002 *Langmuir* **18** 1082
[57] Sear R P 2002 *Phys. Rev.* E **66** 051401
[58] Rotenberg B, Dzubiella J, Hansen J P and Louis A A 2004 *Mol. Phys.* **102** 1
[59] Aarts D G A L, Tuinier R and Lekkerkerker H N W 2002 *J. Phys.: Condens. Matter* **14** 7551
[60] Schmidt M, Denton A R and Brader J M 2003 *J. Chem. Phys.* **118** 1541
[61] Schmidt M and Denton A R 2002 *Phys. Rev.* E **65** 061410
[62] Paricaud P, Varga S and Jackson G 2003 *J. Chem. Phys.* **118** 8525